Biophysical Chemistry 8 (1978) 341–355

RATE-DETERMINING PROCESSES IN THE TRANSPORT OF Pr^{3+} IONS BY THE IONOPHORE A23187 ACROSS PHOSPHOLIPID VESICULAR MEMBRANES. A ^{1}H-NMR AND THEORETICAL STUDY

G.R.A. HUNT and L.R.H. TIPPING
Department of Science, The Polytechnic of Wales, Pontypridd, Mid Glamorgan, CF37 1DL, UK
and
M.R. BELMONT
Department of Engineering Science, University of Exeter, Exeter, EX4 4QF, UK

Received 8 December 1977; revised manuscript received 18 April 1978

Rate constants and activation parameters have been determined for the transport of Pr^{3+} ions by the ionophore A23187 across dipalmitoyl phosphatidylcholine vesicular membranes. The novel method described depends on the measurement of changes in chemical shift of the ^{1}H-NMR choline head-group signals as Pr^{3+} is transported from outside to inside the vesicles. The determined rates are directly proportional to A23187 concentration, suggesting that the rate-determining step involves the species $[Pr(A23187)]^{2+}$. A theoretical analysis of the initial stages of Pr^{3+} transport leads to the conclusion that diffusion over the image potential barrier is the rate-determining step. Calculation of the form and height of this barrier for the non-equilibrium state gives results which agree well with the experimental activation energy and also correctly predict a two-fold reduction in rate of transport when 7 mol % decane is present in the bilayer.

1. Introduction

In order to gain insight into mechanisms by which metal cations are transported across biological membranes, extensive use has been made of the carrier molecules known as ionophores [1–3]. One of these ionophores A23187 [4] is specific for divalent and trivalent ions [5] and has therefore been widely used to study Ca^{2+} transport and function in membranes [6]. However, detailed knowledge of the mechanism of ionophore-mediated transport, even in model membrane systems, is still lacking and there are puzzling discrepancies concerning the stoichiometry of the species involved [7,8].

To attempt to throw further light on some of the possible molecular species and mechanisms of transport we have developed a novel method using high-resolution NMR spectroscopy. It has been shown that ^{1}H, ^{31}P and ^{13}C-NMR can be used to distinguish the inner and outer surfaces of phosphatidyl choline vesicles by adding paramagnetic lanthanide ions to the vesicle solutions [9,10]. Ions such as Pr^{3+} or Eu^{3+} shift the ^{1}H signals from the extravesicular surface of the vesicles leaving the signal from the inner half of the bilayer unshifted. A preliminary publication [11] has indicated that the rate of transport of Pr^{3+} across dipalmitoylphosphatidyl choline (DPPC) vesicular membranes by the ionophores A23187 or X537A can be followed using the time-dependent alterations in the ^{1}H-NMR spectrum.

We now report the details of a considerable improvement in the method (using shift rather than broadening data) from which rate constants and activation energy parameters are calculated. We also report the effect of including n-decane in the phospholipid bilayer in order to relate our work to that based on the Mueller-Rudin type of lipid membrane [12,8]. A detailed theoretical analysis is made of various possible mechanisms for the initial stages of Pr^{3+}-A23187 transport in the light of the experimental data. Good agreement is obtained by postulating that the species transported is $[Pr(A23187)]^{2+}$ and that its diffusion over the image potential barrier is the rate-determining process.

2. Materials and methods

2.1. Chemicals

DL-α-dipalmitoyl phosphatidyl choline (DPPC) and praeseodymium chloride were purchased from Koch Light. The purity of the DPPC was checked by TLC; no traces of lysophosphatidyl choline were seen after sonication procedures. The ionophore A23187 was a gift from the Lilly Research Centre. n-Decane was obtained from BDH.

2.2. Preparation of vesicles

The vesicles were prepared by sonicating 50 mg of DPPC in 2 ml D_2O for 10 minutes at 50-60°C, using a Dawe Soniprobe Type 573A fitted with a microtip, at a setting delivering approximately 25 watts. Under these conditions it has been shown that a homogeneous population of small vesicles is produced, each containig a single lipid bilayer [13]. The DPPC vesicles so formed have consistent average diameters of 26 nm, as deduced from the ratio of the signal areas from the outer and inner phospholipids, which is 1.8 in a large number of our recorded samples. The homogeneity of the vesicles was also checked using electron microscopy of freeze-fractured samples. In order to ensure that the condition of each vesicle sample was similar, they were not allowed to fall below 50°C before commencing the recording of NMR spectra. For the same reason they were not centrifuged, but the sonicator probe tip was repolished after every few sonications, a procedure which avoided contamination by Ti particles from the microtip.

Incorporation of n-decane into the DPPC vesicles was carried out by dissolving weighed amounts of DPPC and n-decane in chloroform, then removing the solvent under a stream of nitrogen, followed by evacuation. The accurate mole % was then based on the final weight of material. The DPPC-decane mixture was then sonicated as above.

2.3. Kinetic experiments

Exactly 1.0 ml of DPPC vesicles in D_2O (prepared as described above) were placed in an NMR tube and inserted in the magnetic field of the spectrometer. A JEOL C-60HL ^1H NMR spectrometer was used,

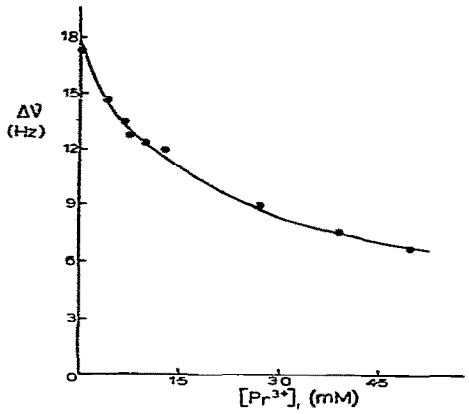

Fig. 1. Calibration graph giving the differences in chemical shift ($\Delta\nu$) between the outer (O) and inner (I) choline ^1H-NMR signals obtained from DPPC vesicles as a function of the concentration of Pr^{3+} ions in the intravesicular region $\{Pr^{3+}\}_i$. Extravesicular Pr^{3+} concentration, $\{Pr^{3+}\}_o$ constant at 5 mM.

fitted with a calibrated temperature control. When the tube reached the desired temperature standard praeseodymium chloride solution was added to the tube so that the concentration of Pr^{3+} ions outside the vesicles reached 5 mM. This was achieved by adding to the vesicle solution 20 μl of a stock solution containing 0.426 mg $PrCl_3 \cdot 6H_2O$ dissolved in 5 ml D_2O. The use of hydrated praeseodymium salt enables an HOD peak to be obtained which is useful in optimising the resolution of the spectrometer. The initial spectrum of the outer O, and inner I, choline head-group signals were recorded. Next, a known concentration of A23187 was added to the same NMR tube in microlitre quantities from a stock solution containing 5 mg of A23187 in 1 ml of absolute ethanol. NMR spectra in the region of signals O and I were then recorded at regular time intervals, and the difference in chemical shift, $\Delta\nu$ between signals O and I noted.

The change in chemical shift difference $\Delta\nu$ is not directly proportional to the concentration of Pr^{3+} arriving on the inside of the vesicles, $\{Pr\}_i$. Hence, in order to determine the rate constants a calibration plot was obtained of $\Delta\nu$ against $\{Pr\}_i$. This was obtained by sonicating DPPC in the presence of varying concentrations of Pr^{3+} and then adding Pr^{3+} ions to the outside of the vesicles so that the total concentration in the

extravesicular region was 5 mM. The calibration plot used in these kinetic experiments is shown in fig. 1. It is important to note that in preparing vesicles containing known concentrations of Pr^{3+} in the intravesicular space, the DPPC was shaken with the D_2O solution of Pr^{3+} at the required concentration for at least one hour at 50–60°C prior to sonication.

Kinetic experiments were carried out at various temperatures between 50°C and 75°C, i.e. above the gel to liquid-crystal transition of DPPC (42°C) and at different concentrations of A23187.

Recently Lawaczeck et al. [14] have reported that DPPC vesicles become appreciably permeable to paramagnetic ions at elevated temperatures. We have held samples of DPPC vesicles at temperatures up to 90° for 3 hours (which is considerably longer than the time scale used in the transport experiments) and there was no change in the signal ratio of signals O/I and no change in $\Delta\nu$. This indicated that the vesicles remained impermeable to Pr^{3+} alone. The discrepancy with Lawaczeck's results cannot be explained but may be due to trace amounts of other lipids, below the concentration detectable by TLC, occurring in the different commercial samples of DPPC used. In any case, Lawaczeck does not observe the gradual downfield shift of signal I, which is characteristic of the ionophore-mediated transport. Rather he observes an increase in signal O and loss of signal I so that a quite different mechanism must be postulated for the presence of Pr^{3+} inside the vesicles. The results reported here thus remain valid since they are concerned *only* with the ionophore-mediated transport of Pr^{3+}.

3. Results

The rate of transport of Pr^{3+} is then determined by measuring the change in chemical shift of the choline signal (I) from the inside of the vesicles. As the ionophore A23187 transports the Pr^{3+} ions from the outside to the inside of the vesicles, the inner peak I is shifted downfield towards outer peak O, as shown in fig. 2. The outer signal O does not shift during transport because of the excess Pr^{3+} in the extravesicular region. Using the calibration plot in fig. 1, the concentration of Pr^{3+} arriving in the intravesicular space $\{Pr^{3+}\}_i$, can be determined.

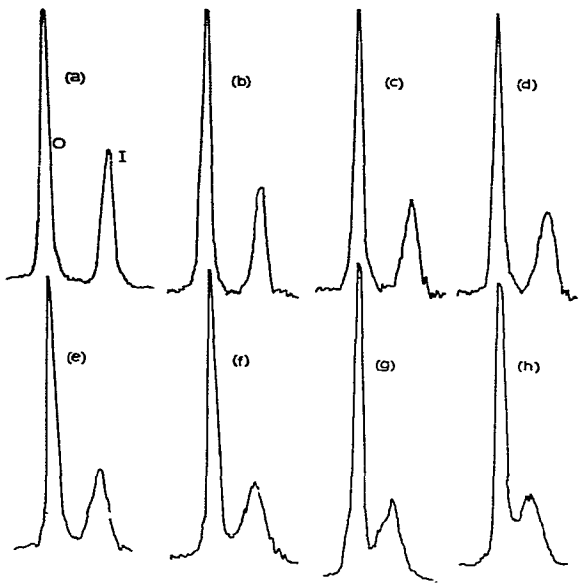

Fig. 2. ^1H NMR spectra at 66°C of the choline signals of DPPC vesicles containing 5 mM Pr^{3+} in the extravesicular region. The spectra show the result of transport of Pr^{3+} into the intravesicular region by A23187 (10 μg/25 mg DPPC) after (a) 0, (b) 2.5, (c) 4.75, (d) 7.25, (e) 10.25, (f) 17, (g) 32.5 and (h) 54 min.

3.1. Rate constants

Plots of $\{Pr^{3+}\}_i$ against time enable the rate constants for transport to be calculated from the slopes of the straight lines obtained. The linearity of the plots during the initial stages of the transport indicates that the rate v, at which Pr^{3+} ions arrive in the intravesicular space is zero order with respect to the intravesicular concentration $\{Pr^{3+}\}_i$. That is, $v = d\{Pr^{3+}\}_i/dt = k$, the zero order rate constant. The extravesicular concentration, $\{Pr^{3+}\}_o$, remains effectively constant at 5 mM since $\{Pr^{3+}\}_o \gg \{A23187\}$. Fig. 3 shows a typical plot of $\{Pr^{3+}\}_i$ against time.

3.2. Activation energy

Rate constants were obtained at various temperatures between 50°C and 75°C, keeping the concentration of the ionophore, {A23187}, constant. The activation energy E_a for the transport of Pr^{3+} was then

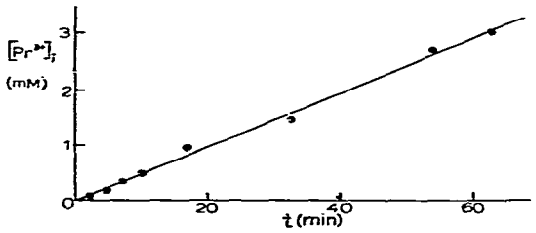

Fig. 3. Kinetic plot of concentration of Pr^{3+} in the intravesicular region $\{Pr^{3+}\}_i$ as a function of time, t, at 66°C for 10 μg A23187/25 mg DPPC. Extravesicular Pr^{3+} concentration, $\{Pr^{3+}\}_o$ = 5 mM.

obtained from the Arrhenius plot and is shown in fig. 4. The value of 116 k J mol^{-1} (27.7 k cal mol^{-1}) agrees quite well with the theoretical prediction.

3.3. Dependence of rate of transport on A23187 concentration

The order of the rate of transport of Pr^{3+} with respect to A23187 was determined from the slope of the straight line obtained by plotting log k_{obs} against log {A23187}. This plot is shown in fig. 5(a) and the slope was found to be 1.1. On plotting k_{obs} against {A23187} a straight line is obtained passing through the origin as seen in fig. 5(b). The rate of transport is hence first order in A23187.

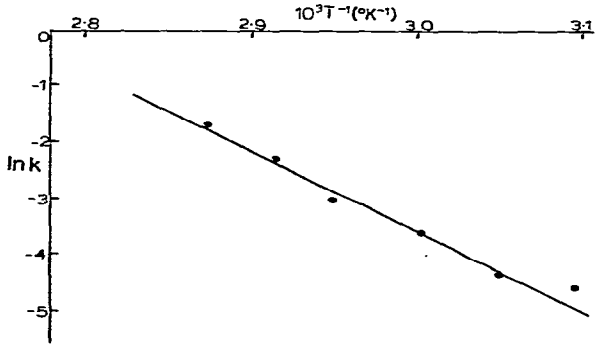

Fig. 4. Arrhenius plot for transport of Pr^{3+} by A23187 (10 μg/25 mg DPPC) with extravesicular Pr^{3+} concentration, $\{Pr^{3+}\}_o$ = 5 mM.

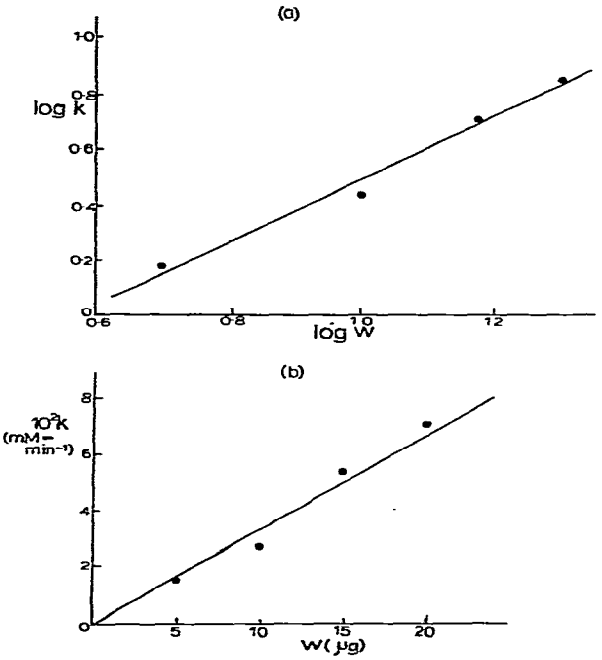

Fig. 5. (a) Plot of the log of the observed rate constants of transport of Pr^{3+} by A23187 through DPPC vesicles at 60°C as a function of the log of the weight of A23187. (b) Plot of the observed rate constants of transport of Pr^{3+} by A23187 through DPPC vesicles at 60°C as a function of the weight of A23187 in micrograms.

3.4. Dependence of rate on presence of decane in the bilayer

The results are summarised in table 1. It is clear that the presence of n-decane considerably lowers the rate of transport. The result is similar to the effect of n-decane on the rate constant of translocation, K_{ms}, for the valinomycin-Rb^+ complex through glycerol-monooleate planar membranes, as reported by Benz et al. [12].

4. Theoretical models

4.1. Which is the rate limiting process?

The theoretical section is devoted firstly to an attempt

Table 1
Rate constants $k_{60°C}$ for A23187-mediated transport of Pr^{3+} across DPPC vesicular membranes compared with values of $k_{60°C}$ obtained using membranes containing 7 mol% n-decane

Concentration of A23187 added outside vesicles	Rate constants, $k_{60°C}$ (m mol^{-1} min^{-1}) × 10^2	
	vesicles containing no decane	vesicles containing 7 mol% decane
10μg/50 mg DPPC/ 2 ml D_2O	2.70	1.63
15μg/50 mg DPPC/ 2 ml D_2O	5.36	2.64

to establish the nature of the rate controlling mechanism for charge transport across the bilayer, and secondly to attempt to model the process.

The Stokes-Einstein relationship shows that vesicles of diameter 26 nm will tumble in dilute aqueous solution at a rate of 10^6 s^{-1}. Thus the effects of unstirred layers and local depletion can be neglected [16]. Initially the possibility will be examined that pure diffusion across the hydrocarbon region, which forms the bulk of the layer, is rate limiting. Although this is readily shown to be impossible the discussion of this point is taken to some length as the results are required later.

4.2. *Pure diffusion control*

The hydrocarbon chain part of the bilayer, henceforth called the residue region, is considered as a bulk *n*-alkane. As the complexed ion is large, one might expect it to be well described by the Stokes-Walden relationship [17]. This states that the magnitude of the measured activation energy ϕ_m for diffusion (and drift mobility) is equal to the magnitude of the activation energy ϕ_v of the shear viscosity of the host medium, which in this case is a bulk n-alkane. For small highly mobile ions there is some departure from the Stokes-Walden relationship and ϕ_m is found to e closer to 1.5 ϕ_v [17,18], but for large low-mobility charge carriers this departure is not observed [19]. So for the large A23187/Pr^{3+} complexes, ϕ_m is expected to be close to ϕ_v. For n-alkanes ϕ_v rises rapidly with chain length, up to ~C_{10}, but above that the rate of increase falls off [17]. The resulting ϕ_m values are much lower than the present measured activation energies. Even for alkanes up to C_{30} the ϕ_m value would only be 16.4 kJ mol^{-1} (3.9 k cal mol^{-1}).

One could possibly argue that the n-alkane description is too over-simplified. After all, the lipid exhibits liquid crystal behaviour [20], so that it is worth while looking at values of ϕ_m measured for organic liquid crystals. Extreme model substances might be MBBA (N-P-methoxybenzylidene-p-n-butylaniline) and CBOA (N-P-cyanobenzylidene-p-n-octylaniline), for which ϕ_m is 29–39 kJ mol^{-1} (6.9–9.2 k cal mol^{-1}) in both the nematic and isotropic states [21,22,39]. For liquid crystals exhibiting a cholestrolic phase the viscosity activation energies do tend to be somewhat higher than for the alkanes [23]. For example, the cholestrylesters of long chain fatty acids, e.g. cholestryl palmitate and cholestrylstearate, have values of about 42 and 50 kJ mol^{-1} respectively. These are still too low to account for the present activation energies. In any case, as with MBBA and CBOA, such substances are extreme case models and the alkane picture of the residue is more realistic.

It is therefore unlikely that pure diffusion through the hydrocarbon region would exhibit a sufficiently high activation energy to be the rate limiting process. Further support for this conclusion comes from White [24] who provides evidence for greater overall mobility within the lipid's hydrocarbon region than would occur in the appropriate bulk n-alkane. This makes it likely that activation energies in the residue region would be even lower than the bulk figures quoted.

It is possible to reach the same conclusion rather more directly by making an upper-limit estimate of the absolute value of the diffusion coefficient D_e needed to explain the present results by a diffusion-controlled process and comparing it with an appropriate alkane diffusion coefficient D_a.

The result for D_e, as would be expected from the comments on activation energies, is many orders of mag

nitude lower than a prediction of the likely diffusion coefficient of complexed ionophores in phospholipids, based on an alkane residue picture. The estimate of D_e is obtained as follows:

The distance λ travelled by diffusing entity in τ seconds is given by

$$\sqrt{D_e \tau} \sim \lambda. \quad (1)$$

Thus the order of time τ_e taken to reach diffusive equilibrium in a vesicle of diameter 200 Å is given by

$$\tau_e \sim (2 \times 10^{-10})^2 / D \text{ s} \quad (2)$$

Eq. (2) errs on the conservative side as it assumes that all the vesicle is composed of phospholipid rather than the less viscous water. In the present experimental situation equilibrium is not easy to define exactly, but certainly has not been reached in a hour. Thus:

$$D_e < \frac{(2 \times 10^{-8})^2}{3.6 \times 10^3} \approx 10^{-19} \text{ m}^2 \text{ s}^{-1}.$$

The estimate of D_a based on viscosity measurement on alkanes combined with the Stokes-Walden relationship mentioned previously [17], leads to $D_a \sim 10^{-12}$ m^2 s^{-1} for charge carriers of the diameter of the complex.

Thus a comparison of the absolute values of D_e and D_a reinforces the argument that pure diffusion across the residue region is not the rate limiting process.

4.3. Diffusion over the image barrier as the rate limiting process

Having concluded that the rate limiting step is unlikely to be pure diffusive transport, the effects of the image potential barrier are now included. The rate limiting step is then assumed to be the diffusion over this barrier of one of the species $[Pr(A23187)]^{2+}$ or $[(Pr(A23187)_2]^{+}$. Initially, the form of the potential barrier is established as follows.

4.4. Models for the barrier and the complex

Owing to electrical forces experienced by a charge near a polar/non-polar interface, the charged complex must do work in crossing the residue region. The presence of the two boundaries forming a single bilayer would result in a symmetrical barrier. However, there is some deformation of the symmetrical barrier produced by the polarisation of the bilayer on the opposite side of the vesicle. (Wall curvature, and its effects, are insignificant over most of the vesicle because of the large relative size of the vesicle compared to the complex.)

The bulk of the treatment of the barrier is presented in Appendix A1 and the general conclusion is that it is justifiable to use as a model an infinite plane slab of non-polar material surrounded by a polar phase. This is also the model generally used for Mueller-Rudin 'black' lipid bilayer transport calculations [12,25,26].

The $[Pr(A23187)]^{2+}$ complex is conventionally modelled by an equivalent composite sphere [25]. The inner core region from the ionic radius to a radius r is assumed to be composed of the polar and hydrogen-bonded groups, while the outer layer from $r \rightarrow a$ corresponds to the non-polar groups (mainly CH_3). These outer groups will have a lower local dielectric constant ϵ_r approximately equal to that of the saturated residue region, i.e. $\epsilon_r \approx 2$. As the available X-ray data on A23187 complexes refers to a crystalline complex with Ca [28] it was necessary to estimate a and r using the appropriate Van der Waals volumes [27].

To determine the charge on the complex, the number of and the state of ionisation of the A23187 units participating is required. Experimentally, the rate constant is proportional to ionophore concentration. Thus the simplest kinetic interpretation is assumed i.e. that one A23187 is unit involved. This is supported by earlier results using the n.m.r. method [11]. Since the ionophore permeates in from the aqueous phase the COOH group is assumed to be ionised so that the most likely net charge on the complex is two fundamental units, corresponding to a species $[Pr(A23187)]^{2+}$. (See also section 5.)

The potential ϕ in fig. 6(a) tends to infinity as $x \rightarrow 0$ and $x \rightarrow 2W$. This is a consequence of the use of ideal abrupt interfaces. Consequently it is necessary to examine the situation where the complex is close to the interface. For convenience the case is considered of a complex moving in the hydrocarbon residue region, towards rather than away from the polar head-groups. A detailed analysis of the behaviour of ϕ when the complex is at or within a distance equal to its own radius from an interface is not feasible since there is

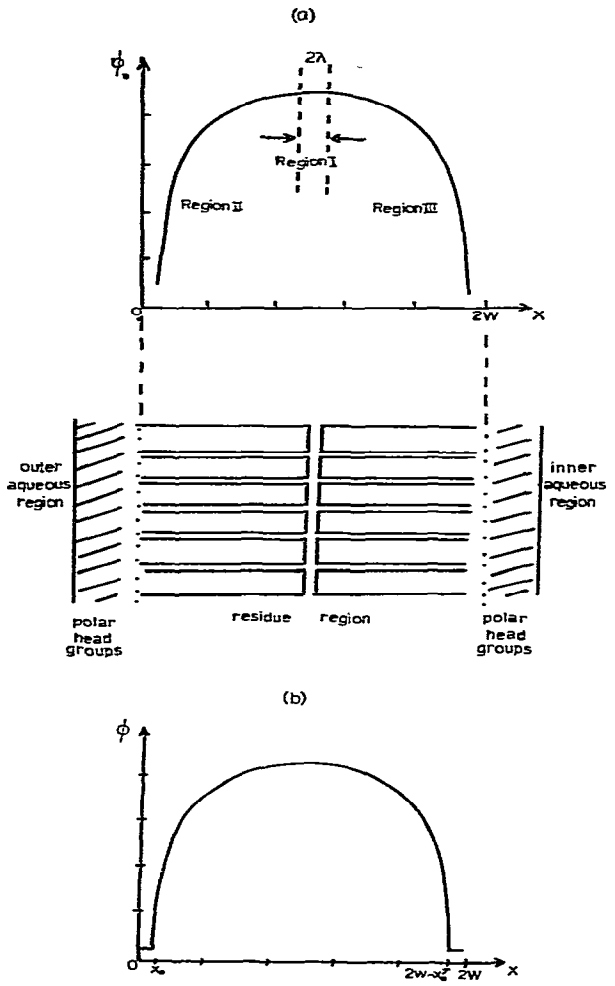

Fig. 6. Image barrier potential ϕ in relation to the bilayer. For significance of regions I, II and III see text. (b) Barrier truncated at x_0 and $2W - x_0$.

not enough information about the complex/interface conformation. The conventional way of overcoming this type of interfacial singularity problem is to use a monotonic function to join the potentials on either side of the interface, joining being done at points where these potentials are known with some confidence. Neumcke and Läuger adopt this approach in their analysis of the steady state conductivity of a black lipid membrane [26]. As an approximation they retain a point-charge expression for the potential of their spherical-ion model to within one ionic radius of the interface. This does not produce a large error in the magnitude of the potential as is shown by comparison with the more realistic sphere model in Appendix A1. (For a single interface the more realistic sphere model and the point potential agree reasonably well up to about 6 Å from the interface.) However, the errors in the derivatives are substantial and would affect the joining function. Neumcke and Läuger estimate the energy of the ion in the polar phase by using the bare ionic radius in the Born model. This neglects the discrete and bound nature of the solvation shell. Examples of the errors in the Born model are given by Moore [29].

The above approach, with some minor modifications would appear to be the sensible one to adopt in the present situation. Unfortunately it is not possible to do so as the errors involved in joining would be far too large. This is because the above analysis [26] treats the case of an ion transferring unchanged from the aqueous region into the bilayer; there are no sudden potential variations involved. While in complete contrast, the present situation involves large changes in the radius and net charge during the transfer. Any attempt to incorporate the resulting abrupt potential changes across the interface would not only be very complicated but would introduce an unacceptably large uncertainty in the potential. To circumvent this problem a rather more physical approach is developed for the present calculations. Basically this method serves to define a truncation point for the image potential; see fig. 6(b).

In general terms one can say that for $x < a$ the gradient of the potential will rapidly tend to zero as the complex begins to enter the polar head-group region. Two effects will be contributing to this. Firstly, the beginning of the entry of the charged complex into the polar phase. Secondly, and superimposed upon this is the positional uncertainty in the location of the complex centre relative to the mean interface. This uncertainty is due to the continuous conformational fluctuations of the highly mobile lipid head-groups. Thus one would expect the potential to flatten out in the region where it is impossible to say with any confidence whether the complex is still wholly in the residue or whether it has begun to enter the polar head-group region. Thus in moving from the

interface to the potential maximum the complex must surmount a barrier $\Delta\phi$ whose lower bound is given by

$$\Delta\phi > \phi(W) - \phi(a) \tag{3}$$

An upper bound to $\Delta\phi$ can be obtained by noting that when the complex centre is $\leqslant r$ from the interface a substantial part of the complex can with some certainty be said to be within the polar head-group region. Irrespective of the details of the process, that part of the complex will be destabilised laying bare the inner polar core. At r this polar core edge is coincident with the mean interface so one is forced to conclude that the core region is now effectively part of the head-group region. This is a sufficient condition to say that the complex has left the residue region.

Thus the potential flattens out at a distance x_0 from the mean polar/non-polar interface somewhere in the range $a \geqslant x_0 \geqslant r$. It seems more likely that x_0 is closer to r because the net charge lies within the central region and the outer non-polar groups are almost indistinguishable from the residue medium. Thus it would appear that a reasonable first approximation for $\Delta\phi$ is

$$\Delta\phi = \phi(W) - \phi(r). \tag{4}$$

4.5. Transport rate calculation

Having established the form of the potential barrier it is now necessary to calculate the flow rate over this into the inner aqueous region.

Under the prevailing experimental conditions the flow into individual vesicles is a highly discrete process rather than a good approximation to a continuous flux which could be treated by conventional continuum transport theory. At the concentration of Pr^{3+} used (5 mM) the equilibrium number of ions within each vesicle is only of the order of 10. However, provided there is negligible interaction between the transporting entities and those already accumulated, one could consider a very large number of equivalent systems and define a continuum ensemble average concentration, n, over the population of vesicles. The non-interaction condition is necessary because otherwise the electric field E will have an additional component arising from the charges which have been already accumulated within the vesicle. Hence this treatment is only valid for the initial stages of transport.

Having defined n one can then set up an equation for the ensemble average flux density, J, within the residue region in terms of drift flux, J_{drift}, and a diffusion flux, J_{diff} where

$$J = J_{\text{diff}} + J_{\text{drift}} \tag{5}$$

or in terms of n

$$J = -D\nabla n + E\mu n \tag{6}$$

and

$$E = -\nabla\phi. \tag{7}$$

Here D is the diffusion coefficient and μ the drift mobility of the complex. The flow process is thus a diffusion migration over the potential barrier defining E.

The planar approximation used in deriving the barrier shape (see Appendix) means that the only spacial variable appearing is x. At this point a formal approach to the problem would involve substituting J_{diff} and J_{drift} into the continuity equation and solving this for $n(x, t)$ subject to the initial and boundary conditions. This is very difficult, partly because of the form of $E(x)$, but mainly because of the rather incompatible nature of the initial condition

$$n(x, 0) = 0 \qquad \text{for } x_0 \leqslant x \leqslant W$$

and the boundary condition at the outer polar interface of the vesicle

$$n(x_0, t) = N_0.$$

This forces one to use a stretched coordinate system near $x = 0$ and use methods similar to those used for boundary layers in fluid mechanics. It was not felt that the system was physically sufficiently precisely defined to warrant such an approach merely for a small-time solution of the problem. This is particularly so because a reasonable approximate solution can be obtained very readily as follows.

Examination of the potential barrier shows that there are three distinct regions (designated I → III in fig. 6(a)). Firstly, the flat top of the barrier, region I, where the electric field strength, E, is very low and consequently the drift flux is negligible; this requires that the flow over the barrier top is diffusion controlled. The width of the region is 2λ, where λ is evaluated

subsequently. Secondly, there is the outer region, II, of the residue, i.e. $W - \lambda > x > 0$. Here the direction of the electric field causes the drift flux to oppose diffusion into the vesicle. This region constitutes the source of the ion flow to the vesicle. Thirdly, there is the inner residue region III, $(2W > x > W + \lambda)$, where the electric field aids the inflow. The field strength increases rapidly towards the inner polar interface at $x = 2W$, sweeping any transporting entities rapidly towards the second polar interface and hence to the inner aqueous region. During the initial stages of transport there is negligible accumulation and consequently the diffusion flux here is insignificant. Thus over most of the range $2W > x > W + \lambda$, one can say with confidence that region III acts as a sink for transporting entities crossing the barrier top and to a good approximation n will be zero there. This conclusion is reinforced by a subsequent argument concerning the order of magnitude of J_{drift}.

Since region III acts initially as a sink then the flux density J into the inner regions of the vesicle will be equal to the diffusive flow over the barrier top which supplies region III. The mean value of J taken over the barrier top is given by

$$J = D\frac{n(W-\lambda) - n(W+\lambda)}{2\lambda}. \tag{8}$$

The problem thus reduces itself to obtaining reasonable estimates for $n(W \pm \lambda)$.

Now it has already been established that over most of region III, $n \approx 0$ and in the next section the value of n in region II is obtained. It then remains to determine how to match the three sections together in order to evaluate $n(W \pm \lambda)$ at the joins.

4.6. Concentration in region II

It was shown in section 2.1 that a pure diffusion-controlled process would lead to equilibrium times vastly too short. In terms of the ensemble average fluxes this means that the diffusion flux J_{diff} would be enormously larger than the net flux. An alternative to using the $\sqrt{D\tau}$ argument of section 2.1 is to use N_0/W as a very coarse order of magnitude estimate of $\langle \partial n/\partial x \rangle$. This leads to the same conclusion. Remembering that in region II J_{drift} and J_{diff} act in opposition, one must conclude from equation (5) that to a very good approximation over most of the outer part of the bilayer (region II)

$$J_{\text{drift}} + J_{\text{diff}} = 0. \tag{9}$$

Thus the transport is a quasi-static process. Eq. (9) enables eq. (6) to be integrated immediately yielding

$$n(x) = N_0 \exp\frac{\mu}{D}\int_{x_0}^{x} E\,dx \tag{10}$$

which is simply the Boltzman distribution in terms of the concentration N_0 at $x = x_0$ and the electrical potential $-\int_{x_0}^{x} E\,dx$. This is more recognisable if one uses the Einstein relationship [17,18] to obtain

$$n(x) = N_0 \exp\frac{-\{\Delta\phi(W)q\}}{kT} \tag{11}$$

4.7. Concentration in region III

In this region diffusion and drift aid each other rather than act in opposition and hence neither of their contributions can exceed the measured flux. Thus to the same order of approximation as in section 4.6 $J_{\text{drift}} \approx J_{\text{diff}} = 0$, which implies $n \approx 0$ within region III, and reinforces the previous arguments about this region.

4.8. Width, 2λ, of the diffusion controlled region I

The next step is to calculate the width, 2λ, of the central diffusion region. The upper limit to λ is determined by the point at which the mean drift rate is equal to the mean diffusion rate. It can easily be shown that this occurs when the electrical work done in travelling a distance λ equals kT, thus applying this criterion to diffusion from $W \pm \lambda$ to the barrier top gives

$$\phi(W) - \phi(W \pm \lambda) = kT \tag{12}$$

from which λ can be either calculated from equation (A2) or determined from the potential plot.

4.9. Calculation of the concentrations at the end points of diffusion-controlled region

It now remains to determine how to use the solutions obtained for the bulk of regions III and II to calculate the concentrations $n(W \pm \lambda)$ at the region III

concentration breaks down within a few kT of the barrier top at $(W - \lambda)$, defined by equation (12), that is, just at the required point. However, this can be readily resolved by approximating the shape of the potential barrier over the top few kT by linear segments. The slope of the segments gives the field value in each segment. (As the barrier height is large with respect to kT and in any case the experimental error is substantially greater than kT, such an approximation is justified.) The section spanning the barrier top is given zero slope, which makes J_{drift} also zero. The first sections in regions I and III then have slopes of $\pm E_1$ respectively and consequently have finite drift terms. If $\partial\phi/\partial x$ increases rapidly enough for $x < W - \lambda$ and $x > W + \lambda$ then E_1 is large enough to justify using the bulk region I and III solutions over these segments. Similarly, $\partial\phi/\partial x$ should fall off rapidly for $x > W - \lambda$ and $x < W + \lambda$ towards $x = W$ to justify the pure diffusion solution there. Provided one is prepared to allow an error of one or two kT in the barrier top value this requirement can always be fulfilled by the process of slicing off the barrier top. In any case expanding ϕ to the first few terms in a Taylor series about W shows that the potential barrier itself satisfies these requirements quite well.

In this linear segment approximation the solutions used are valid right up to the joint point where E changes discontinuously. Continuity of n then forces $n(W \pm \lambda)$ in region I to take on the values defined by the region II and III solutions at these points.

The above argument has a valuable by-product in that it removes some of the arbitrariness in λ. For the more rapidly the potential varies either side of λ the more compressed is the distance over which the drift flux tends to zero and consequently the more precisely λ is defined.

Thus one finally arrives at the following expression for J the flux density into the inner aqueous region:

$$J = \frac{D}{2\lambda} N_0 \exp \frac{-q\{\Delta\phi\}}{kT} \tag{13}$$

In eq. (13) N_0 is the concentration at x_0.

The quantity observed experimentally is not J but an NMR shift which is initially proportional to the concentration n_i within the inner aqueous region close to the inner polar groups. On the experimental time scale over the population as a whole diffusion equilibrium will exist within this inner region, so n_i is given by

$$\partial n_i/\partial t = \partial \{\int_s J \cdot ds\}/\partial V \tag{14}$$

where s indicates integration over the surface of the inner aqueous region and V is the volume. Evaluating (14) for the experimentally observed spherical geometry of the vesicles produces

$$\partial n_i/\partial t = 3J/R,$$

where R is the vesicle radius. Hence using (13), the initial rate v is

$$v = \frac{3D}{2R\lambda} N_0 \exp \frac{-q\{\Delta\phi\}}{kT}. \tag{15}$$

The process responsible for N_0 have been assumed not to be rate limiting, i.e. quasi-equilibrium has been assumed for them. This demands that N_0 will reflect the same dependence on the concentration of A23187 as the experimental rate constant, i.e.

$$N_0 = C_1 I, \tag{16}$$

where C_1 is the A23187 concentration and I the equilibrium constant. Thus the final form of the initial rate v is predicted as

$$v = \frac{3D}{2R\lambda} C_1 I \exp \frac{-q\{\Delta\phi\}}{kT}. \tag{17}$$

5. Comparison with experiment

5.1. Activation energy

The total activation energy which would be exhibited by eq. (17) is given by

$$W_T = W_D + W_I + q\Delta\phi, \tag{18}$$

where W_D is the diffusion activation energy and W_I is the activation energy for the complexation steps. An estimate of W_D based on the bulk alkane values discussed earlier puts in it the range $2.9 \rightarrow 6$ kcal mol^{-1}. It has been assumed throughout that I is definitely not the rate determining parameter and hence to comply with this assumption W_I cannot be a large fraction of W_T. Further supporting evidence for this assumption is to be found in the high rates at which the rare earths undergo complexation reactions in general [30,31]. If I was dominant (e.g. if

complexation were the rate determining step), then transport would be controlled by a spatially localised reaction which can be described by transition-state theory [15]. Using the experimental value of the activation energy $E_a = 116$ kJ mol^{-1}, and the experimental rate constant $k_{60°C} = 2.70 \times 10^{-2}$ m mol l^{-1} min^{-1}, the calculated entropy of activation is $\Delta S_I = 0.0$ J K^{-1} mol^{-1}. It seems extremely unlikely that if processes involving I were dominant then ΔS_I would be close to zero. Thus it will be assumed that to within experimental error W_I is negligibly small, so:

$$W_T = q\Delta\phi + W_D. \quad (19)$$

Inserting the experimental activation energy for W_T and assuming W_D to be somewhere within the range specified above, this requires that $q\Delta\phi$ should be 91 to 103 kJ mol^{-1} (22 to 25 k cal mol^{-1}).

For the single A23187 unit per Pr^{3+} ion, which the experimental results indicate, a Van der Waals volume calculation produces an equivalent mean complex radius of 6 Å. The non-polar outer shell consists mainly of the methyl groups. So subtracting this group radius of 2 Å one obtains an inner polar shell radius of 4 Å. If, as indicated earlier, this inner-shell radius is used to determine the point where the potential gradient becomes zero, in fig. 6(b), one obtains a predicted value for $q\Delta\phi$ of 114 kJ mol^{-1} (27 kcal mol^{-1}). The calculation is performed by substituting the above value for the inner polar shell radius into eq. (4) which is then evaluated by eq. (A.2). The degree of agreement between this prediction and the required mean value, 97 kJ mol^{-1}, is probably fortuitously close. However, even if the agreement had rather been worse, this value justifies the assumption made about W_I. Thus the modelling assumptions appear to be self-consistent.

Despite the good agreement with the experimental activation energy no attempt has been made to estimate the actual value of the rate v. As with all models involving calculations of large activation energies, eq. (17) is very sensitive to the error bound on the exponent $\Delta\phi q/kT$. Adding to this the very coarse approximations which would be made for the other unknown parameters it is easily possible for the predicted range of confidence in v to span many orders of magnitude.

5.2. Concentration dependence

As the initial flow rate is predicted by equation (13) to be directly proportional to N_0 the model exhibits the observed concentration dependency on A23187. It is interesting that Wulf and Pohl, in their study [8] of Ca^{2+} transport by A23187 in planar membranes also report a concentration dependence of A23187 consistent with a 1 : 1 complex. They found this result difficult to reconcile with their observation that transport was electrically silent, indicating the $Ca(A23187)_2$ complex. Co-transport of anions or protons may be involved. In experiments to be reported elsewhere in full it has been found (G.R.A. Hunt, L.R.H. Tipping and M.R. Belmont, unpublished results) that on incorporating the A23187 into the vesicle bilayers during their preparation, the transport data is then consistent with a carrier species $[H(A23187)_2]^-$, instead of $[A23187]^-$.

5.3. Dependence on n-decane in the bilayer

Experimentally it is found that addition of 7 mol % decane to the lipid prior to sonication causes a reduction by a factor of 2 in the measured rate constant (table 1).

The most energetically favourable location for the decane is in the middle of the residue region with a preferred orientation colinear with the residue chains. This has the effect of fluidising both halves of the bilayer, lowering the gel to liquid-crystal transition temperature [32]. This will also affect the bulk residue properties and increase the barrier height by increasing the bilayer width.

The coarsest estimate of the bilayer expansion is obtained by assuming an isotropic volume increase. However, this ignores the expected preferred orientation of the decane. A more realistic approach is to assume that the presence of a decane molecule between opposing lipid molecules can further separate them by a distance δ, which ranges from zero to one decane chain-length. If there was a decane molecule associated with every pair of opposing lipid molecules then the bilayer would uniformly expand by δ, while at lower decane concentrations it is expected there would be local fluctuations up to a maximum of δ. However, the lipid is highly mobile above its liquid-crystal temperature and the decane level is not low, so the

Table 2
Predicted reduction in rate constant due to the raising of the energy barrier by bilayer expansion, δ, in presence of 7 mol % of n-decane

δ/decane length	Fractional reduction in rate constant
0	1
0.19	0.8
0.37	0.7
0.55	0.5
0.74	0.4
1.0	0.3

transporting charges should see a uniform increase in bilayer thickness. This will be approximately equal to $\delta\bar{P}$. Here $\bar{P}$ is the mean chance of finding a decane molecule between a pair of opposing lipids and should be roughly equal to twice the mol fraction of the decane, i.e. 0.14 in the present case.

The predicted reduction in the rate constant produced by the bilayer expansion is given in table 2 as a function of δ/decane length.

As well as affecting barrier height the decane will increase λ and R and modify the residue region diffusion coefficient D. The effect on diffusion coefficient is difficult to assess quantitatively, particularly in view of the expected preferred orientation of the decane. However, the effect is likely to be negligibly small. This can be shown by adopting the coarse isotropic volume increase approach and applying the mixing index technique [33] to the component viscosities [34]. The change in overall viscosity can then be made to yield the change in D by using the Sokes-Walden mobility relationship and the Einstein formula. The resulting change is of the order of 1%, thus a more precise approach seems unjustified as the effect is negligible.

Similarly the effect on the potential barrier of the small change in permittivity produced by decane addition at 7 mol % also has a negligible effect on the rate constant.

Thus the dominant effect should be the barrier height variation. Table 2 shows that the range of possible variation certainly spans the experimentally observed factor of 2 rate reduction. The actual predicted δ value for this reduction corresponds to 0.55 of a decane chain length. (In other words, at addition levels of one decane molecule to each pair of opposing phospholipids the bilayer should expand by 0.55 of a decane length.) There are very good reasons to expect this rather large expansion. Consider the forces acting on the bilayer in equilibrium. There will be a tendency to expand deriving from the hydrophilic nature of the polar head-groups; this is balanced by the work required to produce any separation of the hydrocarbon tails. Any such separation of these tails will lower the local permittivity in the mid-layer region. However, if the local permittivity could be prevented from falling in this way then far less work is required to expand the layer. The presence of the decane in this region with its expected preferred orientation will do just this. The residue chain ends can then readily move along the decane molecules allowing a substantial increase in the equilibrium bilayer width. The expansion would cease when the decane and residue chains came close to separation. When the thermal deformation of a straight decane molecule is allowed for the predicted value of 0.55 of a decane chain for the expansion parameter seems reasonable from this point of view.

Further support for these arguments comes from the large variation in black lipid bilayer widths reported for solvent-free membranes and those containing residual decane solvent [35,36]. The factor two thickness variation would require approximately 10 decane molecules per phospholipid if one adopted a mechanical volume swelling view. Such a large decane concentration makes one question whether such a system would be stable without further thinning. The present model however requires only 3 decane molecules per lipid to achieve the same thickness increase.

6. Conclusion

The model based upon rate limitation by diffusion over the image potential barrier appears to be both qualitatively and, to a large extent, quantitatively successful in describing the initial stage of A23187 promoted Pr^{3+} transport into dipalmitoyl lecithin vesicles.

Thus the initial translayer migration mechanism appears to have been established. However, to describe later stages of transport one needs to consider several further factors. These revolve around the ac-

cumulation of transported ions within the vesicle. Qualitatively the effect is to build up a space charge field opposing the flow. It can be shown that to achieve any significant fraction of the external concentration an equilibrium counter-charge flux of some other species must occur (positive out or negative in). The problem then becomes a multi-carrier flow. (OH^-, H^+, electrons, Cl^- are all possibilities.) [8]. The problem is severely aggravated by the highly discrete nature of the transport. The ensemble average arguments break down as soon as ion-ion interactions become important within individual vesicles. Only when the entities become large enough for continuum concentrations to be meaningful within each vesicle can the continuum transport equations be applied, such as at the level of actual biological cells.

Appendix

Image potential calculation

The model of the phospholipid bilayer is the conventional one of a non-polar residue bounded by a highly polar medium on either side.

The potential ϕ_1 of a point charge, q, at a distance, x, from the interface between two dielectrics of permittivity ϵ_1 and ϵ_2 is given by:

$$\phi_1 = \frac{q\alpha}{4\pi\epsilon_1 2x}\frac{(k-1)}{(k+1)} + \phi_0, \qquad \text{(A.1)}$$

where $k = \epsilon_2/\epsilon_1$ and ϕ_0 is the arbitrary constant potential. Eq. (A.1) can be viewed as the potential of q in the presence of an image charge $q(k-1)/(k+1)$ at $-x$ relative to the interface.

Using this result the method if iterated image charges can be used [40], to calculate the total potential ϕ of the charge within a layer of thickness $2W$:

$$\phi = \frac{q\alpha}{4\pi\epsilon_1 2x}\sum_{n=0}^{\infty}\alpha^{2n} \times \frac{2\alpha}{\beta(n+1)} - \frac{(2n+1)\beta}{(\beta n+1)\{(n+1)\beta-1\}} + \phi_0, \qquad \text{(A.2)}$$

where $\alpha = (k-1)/(k+1)$ and $\beta = 2W/x$. (Note: n is not simply the image number.) Having obtained this result it was discovered that a similar analysis had been previously performed [26], although this is presented in a rather different form to equation (A.2).

The problem of a charged complex in the residue region of a vesicle is more complicated than the previous situation. Three main difficulties arise. Firstly, the complex is not a point charge on the relevant size scale when it is near an interface. Secondly, the interface is not an abrupt change in a continuum, and in addition it continuously fluctuates. Thirdly, the layer in the vesicle is part of an enclosure wall and is not an infinite plane.

Initially, the problem of the structure of the complex is considered. Far from either interface, i.e. close to the mid-layer position, the point-charge approximation will hold because $2W \gg a$. However, close to the interface one would expect that a more realistic picture is needed. In the text the complex has been modelled as a composite sphere whose inner region has a higher polarizability than the outer one. The next simplest approximation to a point charge for such a structure is a conducting sphere of radius r carrying the charge q and this will now be considered. This approximation is valid because the boundary conditions on the electric displacement vector for a polar to non-polar interface are similar to those for a metal interface. Thus, to a first approximation, the situation can be modelled by a charged conducting sphere approaching an infinite conducting plane. The boundary condition arguments apply very well to the highly polar/non-polar interface. (There is no need to consider the effects of the far interface at small x.) The sphere/plane potential can be obtained by using the symmetry plane in the classical two-sphere problem.

A complete solution of the Laplace equation for the two-sphere problem is available as an infinite set of orthogonal functions [37]. However, the convergence of this solution is very poor for small sphere separations which is precisely the situation of interest here. Fortunately, however, a good approximation exists for this case [38]. The resulting potential difference ψ between the sphere and the plane is given by

$$\psi = \frac{2q}{r\{\ln(r/2x) + 2\gamma + 2(\ln 2)\}}, \qquad \text{(A.3)}$$

where γ is Euler's constant (0.577216). It is interesting to note that over the range where (A.3) holds, i.e. $2x/r \ll 1$, there is not a dramatic departure from

Table 3.
Variation in the ratio of the sphere/plane potential (ψ_S) to the point/plane potential (ψ_P) with the ratio x/r, where x is the distance between the charged conducting sphere, radius r, and the infinite conducting plane.

x/r	ψ_S/ψ_P
0.1	1.06
0.05	0.87
0.01	0.62

the point/plane expression until $2x/r$ is very small indeed. The few values given in table 3 illustrate this point. Thus as the sphere model is in any case unlikely to be sufficiently realistic to give a valid description at a very small complex/interface separation there seems to be little point in discarding the simple point-charge model. In any case the potential as used in the text is truncated at $x = r$. It should be noted, however, that over the range x/r from table 3 the first and higher order derivatives of the potential ratio increase rapidly. This obviously presents problems when using the joining function method mentioned in the text.

The second problem which concerns the nature of the interface is dealt with in the main text.

Finally, the boundary geometry problem is considered. The system discussed so far is a single planar infinite non-polar dielectric layer in a highly polar medium. In reality the vesicle is spherical. A complete solution of this problem is difficult. It cannot be tackled by image methods because one of the boundaries is "inside-out" in terms of the equivalent images referenced to one of the media; this can only be resolved by satisfying two boundary conditions simultaneously. To do so means the "geometric optics reflection" property of the images is lost, thus destroying most of the value of the method. Alternatively, a direct solution of Laplace's equation would involve joining across four boundaries which gives rise to a very complicated set of equations for the eigen-values.

For these reasons it was decided to use the single-slab approximation and calculate the magnitude and sign of the maximum possible error. This occurs when the second layer has the most effect, i.e. when the two layers are touching. The intervening polar region is then absent and the problem reduces to the single-layer one, but this time $4W$ wide with the complex moving from x_0 to W. (The barrier maximum in the two-layer case will be shifted somewhat from W by the effect of the second layer, but this is ignored.) For the 40 Å residue regions considered the resulting change in barrier height is an increase by 3.3 kcal mol^{-1}. As this is very much a worst-case condition, it appears to be safe to neglect the effects of the far boundary as the measured activation energies are ~30 kcal mol^{-1}.

References

[1] P. Läuger, Science 178 (1972) 24.
[2] G. Eisenman (ed.) Membranes – A Series of Advances, Vol. 2 (Marcel Decker, N.Y., 1973).
[3] D.H. Haydon and S.B. Hladky, Quart. Rev. Biophys. 5 (1972) 127.
[4] M.O. Chaney, P.V. Demarco, N.D. Jones and J.L. Occolowitz, J. Amer. Chem. Soc., 96 (1974) 1932.
[5] D.R. Pfieffer, P.W. Reed and H.A. Lardy, Biochemistry 13 (1974) 4007.
[6] A. Gómez-Puyou and C. Gómez-Lojero, in: Current topics in bioenergetics, D. Rao Sanadi (ed.), Vol. 6 (Academic Press, 1977) p. 222.
[7] G.D. Case, J.M. Vanderkooi and S. Scarpa, Arch. Biochem. Biophys. 162 (1974) 174.
[8] J. Wulf and W.G. Pohl, Biochim. Biophys. Acta 465 (1977) 471.
[9] P.W. Nolden and T. Ackerman, Biophysical Chemistry 4 (1976) 297.
[10] W.C. Hutton, P.L. Yeagle and R.B. Martin, Chem. Phys. Lipids 19 (1977) 255.
[11] G.R.A. Hunt, FEBS Lett. 58 (1975) 194.
[12] R. Benz, O. Fröhlich and P. Läuger, Biochim. Biophys. Acta 464 (1977) 465.
[13] J.A. Berden, R.W. Barker and G.K. Radda, Biochim. Biophys. Acta 375 (1975) 186.
[14] R. Lawaczeck, R. Blackman and M. Kainoshe, Biochim. Biophys. Acta 468 (1977) 411.
[15] K.J. Laidler, Chemical kinetics (McGraw-Hill, N.Y., 1970).
[16] S. Ciani, F. Gambale, A. Gliozzi and R. Rolandi, J. Membrane Biol. 24 (1975) 1.
[17] I. Adamcyewski, Ionisation, conductivity and breakdown in dielectric liquids (Taylor and Francis, 1969).
[18] M.R. Belmont and P.E. Secker, J. Phys. D: Appl. Phys. 4 (1971) 956.
[19] M.R. Belmont and P.E. Secker, J. Phys. D: Appl. Phys. 5 (1972) 2212.
[20] D. Chapman, R.M. Williams and B.D. Bladbrooke, Chem. Phys. Lipids 1 (1967) 445.
[21] R.S. Porter and J.F. Johnson, J. Appl. Phys. 23 (1963) 51.

[22] K. Yoshimo, Y. Tabuchi, S. Hisamitsu and Y. Inuishi, Proc. 4th Int. Conf. on Conduction and breakdown in dielectric liquids (Typografia Hiberniai, Dublin, 1972).
[23] R.S. Porter and J.F. Johnson, J. App. Phys. 34 (1963) 55.
[24] S.H. White, Nature 26 (1976) 421.
[25] A. Parsegian, Nature 221 (1969) 844.
[26] B. Neumcke and P. Läuger, Biophys. J. 9 (1969) 1160.
[27] L. Pauling, The nature of the chemical bond, 3rd Edn. (Cornell Univ. Press, 1960).
[28] M.O. Charey, N.D. Jones and M. Debono, J. Antibiot. 29 (1976) 424.
[29] W.J. Moore, Physical chemistry, 5th Edn. (Longmans, 1974).
[30] M. Eiger, Pure and Appl. Chem. 6 (1963) 105.
[31] H.D. Bennet and B. Caldin, J. Chem. Soc. A (1971) 2198.
[32] G.R. Hunt and L.R.H. Tipping, Biochim. Biophys. Acta 507 (1978) 242.
[33] J.B. Maxwell, Data Book on Hydrocarbons (Van Nostrand, 1960).
[34] F.D. Rossini, K.S. Pitzer, R.L. Arnett, R.N. Brown and E.C. Pimentel (eds.), Selected values of physical and thermodynamic properties of hydrocarbons and related compounds (Carnegie Press, 1953).
[35] R. Benz, O. Fröhlich, P. Läuger and M. Montal, Biochim. Biophys. Acta 394 (1975) 323.
[36] R. Benz and P. Läuger, J. Membrane Biol. 27 (1976) 171.
[37] P. Moon and D.E. Spencer, Field theory for engineers (Van Nostrand, 1961).
[38] A. Russell, Proc. Phys. Soc. Lond. 36 (1922) 10.
[39] R.S. Porter, E.N. Barrall II and J.F. Johnson, J. Chem. Phys. 45 (1966) 1452.
[40] B.H. Chirgwin, C. Plumpton and C.W. Kilmister, Elementary electromagnetic theory, Vol. 2 (Pergamon 1973).